Persistence of Outgoing Longwave Radiation Anomalies in the Tropics

BRANT LIEBMANN, M. CHELLIAH AND H. M. VAN DEN DOOL

Cooperative Institute for Climate Studies, University of Maryland, College Park, Maryland

(Manuscript received 7 March 1988, in final form 26 September 1988)

ABSTRACT

We examine the persistence of outgoing longwave radiation (OLR) anomalies in the tropics on many different time scales during 1974–86. We calculate "one-lag autocorrelations" by constructing nonoverlapping 1-, 15-, and 60-day averages and calculating the correlation at every grid point between every time average and the following average for the entire dataset. One-day averages produce the largest local autocorrelations everywhere except over the equatorial Pacific. Large autocorrelations using 15-day averages are confined to the equatorial Pacific, but large autocorrelations based on 60-day averages extend eastward from the eastern Indian Ocean through South America. We attribute the increase in autocorrelation in some areas as the averaging period increases to the presence of the 30–60 day oscillation in those areas. The spatial match between the autocorrelation and the standard deviation of OLR is best for 60-day averages and worst for 15-day averages.

We then calculate pattern correlations over a domain that extends along the equator from the eastern Indian Ocean through the central Pacific. When plotted as a time series the one-lag pattern correlations for two-month means are seen to vary wildly, although they are generally positive. There are some extended periods, however, during which the pattern correlation remains large, most notably during the 1982–83 ENSO event.

The average one-lag pattern correlation is plotted for many different time averages. They decrease until a minimum at 20-day averages, beyond which they slowly increase as the averaging length is increased.

The average one-lag pattern correlations using one-day averages are smallest during the mid-year months, but using 60-day averages they are largest during these months. The seasonality, however, is not large.

Finally, we identify eastward propagation of OLR anomalies with at least two distinct phase-speeds in addition to a quasi-persistent signal. It is suggested that forecasts of OLR anomalies might be improved over simple, local persistence by a multiple regression technique.

1. Introduction

If one accepts the celebrated hypothesis that anomalous latent heating in the tropics influences the midlatitude standing-wave pattern, then an advance knowledge of that heating distribution would be useful. The purpose of this paper is to present results of a study examining the persistence of tropical outgoing longwave radiation (OLR) anomalies, which are intended as a proxy for latent heat release, at many different time scales.

Specifically, we are attempting to answer the following questions: 1) Are there any time scales and/or locations that are clearly best for prediction of OLR anomalies by persistence? We consider autocorrelations that are made from averages of one day to several months. 2) Is persistence a function of time of year? 3) Can a systematic propagation of OLR anomalies be detected from the lag-correlations? If so, then forecasts of OLR anomalies might be improved over local persistence of the initial anomaly.

Corresponding author address: Dr. Brant Liebmann, University of Colorado at Boulder, Cooperative Institute for Research in Environmental Sciences, Campus Box 449, Boulder, CO 80309-0449.

2. Data

Twice-daily OLR data on a 2.5 × 2.5 degree grid were obtained from the NOAA operational satellites. We used data from June 1974 through February 1986, excluding mid-March through December 1978. All missing data (except the huge gap in 1978) were replaced by a linear interpolation in time at each grid point for both day and night separately. If two or more consecutive measurements were missing, data from the nearest observations before and after the missing observation were averaged, with weighting inversely proportional to their time from the missing observation. We thus obtained a complete map from 45°N to 45°S for every day and every night of the record, which were then combined to form daily averages.

Determining the climatology that should be removed in order to construct anomalies is never trivial. It is an especially important consideration in studies involving autocorrelation because an incorrect climatology can result in false autocorrelations. A thorough discussion of the method we used to compute a climatology is presented in appendix A, but the method is briefly described below.

We first formed calendar month normals by averaging monthly means. We then Fourier analyzed the monthly normals at each gridpoint to obtain the annual

and semiannual harmonics, and subtracted these and the annual mean from every day of the record.

Since the OLR field is noisy in space, we smoothed each daily anomaly field by retaining only the zonal mean and the first ten zonal harmonics at each latitude, and then filtered each field twice with a 1–2–1 filter in the meridional direction. Thus, we are left with a series of daily maps of deviations from climatology that represent the large-scale anomalous cloudiness pattern, which we hereafter refer to as "anomalies."

3. Results

a. Local autocorrelations and standard deviations at individual gridpoints

One-lag autocorrelations are calculated at every gridpoint for different averaging lengths. Briefly, the one-lag autocorrelation is defined (see appendix B for a thorough definition of "autocorrelation") as the covariance of a particular average with the subsequent nonoverlapping average over the dataset and divided by the variance of those averages. It should be noted that usually the "skill" of forecasts based on one-lag autocorrelations of time averages comes mainly from the correlation between the last few days of the antecedent period and the first few days of the subsequent period (Roads and Barnett 1984).

The one-lag autocorrelations for anomalies based on 1-, 15-, and 60-day averages are shown in Fig. 1. Daily averages include synoptic variability, 15-day averages filter the high frequencies while still retaining low-frequency intraseasonal variability, and 60-day averages act as the shortest filter that approximately eliminates the 30–60 day oscillation. The data are pooled here to include all years and seasons. The pattern of one-day autocorrelations (Fig. 1a) is quite different from that for the longer averaging periods, even though the variance of the longer periods is contained in the one-day averages, indicating that much of the total variance is found in the shorter periods. One-day autocorrelations (Fig. 1a) which exceed 0.8 are found over much of the Indian Ocean and over the central Pacific south of the equator. The one-day autocorrelations clearly diminish toward high latitudes. One-lag autocorrelations from daily data that were not spatially filtered (not shown) are quite similar to those using filtered data, except that the contours are more noisy, and in general the autocorrelations are 0.1 to 0.15 lower than in the filtered data.

The one-lag autocorrelations made from 15-day averages (Fig. 1b), exhibit a near "bulls-eye" centered on the equator over the central and eastern Pacific, and little autocorrelation elsewhere.[1] The 60-day autocorrelation map (Fig. 1c) shows a pattern similar to the 15-day map, but is more extensive, with lobes of high correlation extending eastward through South America and westward through Indonesia.

We attribute the differences between the 1-day and 15-day autocorrelations to the averaging out of individual synoptic "events." The pattern made with 15-day averages looks suspiciously like the signature of the 1982–83 El Niño/Southern Oscillation (ENSO) event. Maps made by omitting 1982 and 1983 from the record (although we did not recalculate the climatology) reveal the pattern in Fig. 1b to have moved somewhat westward, although the largest autocorrelations still occur east of the dateline.

We believe the differences between the 15-day and 60-day autocorrelation maps are due to the presence of the 30–60 day oscillation, which is active over the western Pacific and Indonesia as well as South America, at least in the Northern Hemisphere (Weickmann et al. 1985). An oscillation with a period between 30 and 60 days would significantly reduce positive (or produce negative) autocorrelations using 15-day averages.

The standard deviations of 1-, 15-, and 60-day average anomalies are presented in Fig. 2. The largest values occur near the equator over the central and western Pacific on all maps, and over the Indian ocean on the 1- and 15-day maps. Small standard deviations for all three time averages are evident in the Southern Hemisphere west of Africa, South America, and to a lesser extent, Australia. Standard deviations from daily averages that were not spatially filtered are like the filtered version except that the values of the former are 15 to 20 percent higher.

The correlation between the spatial patterns of the standard deviation and the autocorrelation, averaged between 15°N and 15°S, is 0.44, 0.09, and 0.65 for 1-, 15-, and 60-day averages, respectively. Again, the 30–60 day oscillation is to blame for the poor spatial match at 15-day averages, since it contributes significantly to the total variance at many points, but is also responsible for the low 15-day one-lag autocorrelations at those points. Thus, using 15-day averages, this implies that forecasting by simple, local persistence will not work particularly well in areas where variations of OLR are greatest. In general, however, for a stationary red-noise process one expects locations with large autocorrelation to be associated with a large variance provided that the random perturbation has the same variance at every gridpoint (Van den Dool and Chervin 1986).

To answer the question of whether there are preferred time scales or locations for persistent OLR anomalies we distinguish three regions. 1) All areas except the equatorial Pacific: The one-day time scale is by far the best for simple prediction. 2) The equatorial Pacific: The success of persistence is less dependent on time scale, meaning that 60-day means (centered 30 days into the future) are as predictable as one-day means. 3) Indonesia and South America: Although

[1] The secondary maximum in the autocorrelation field over the Sahara is probably due to a linear trend associated with changes in the equatorial crossing times of the satellites (Dr. J. S. Winston, personal communication).

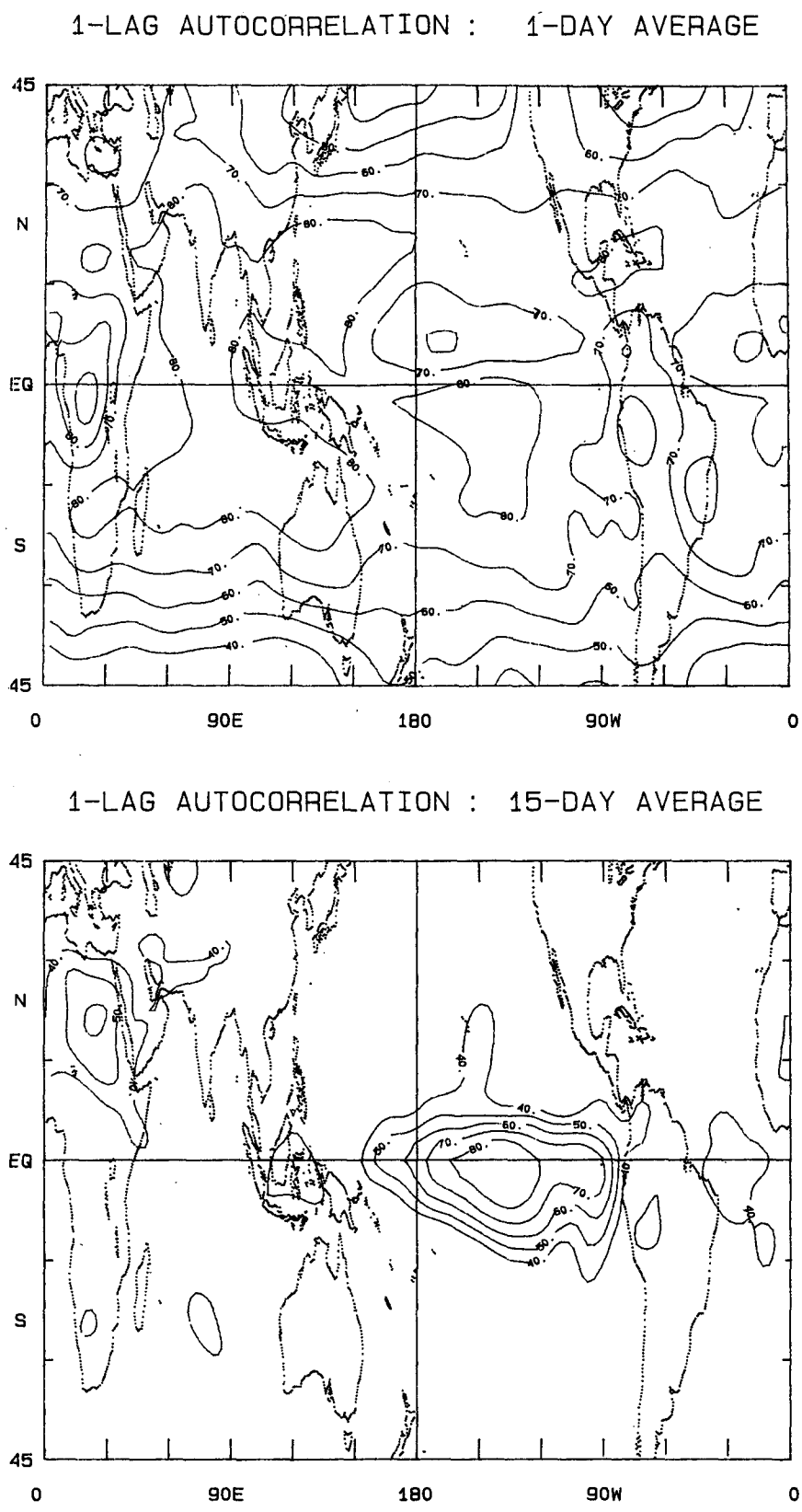

FIG. 1. One-lag autocorrelation of deviations from the seasonal cycle of OLR for (a) 1-day, (b) 15-day, (c) 60-day averages. Contours are plotted in percent at intervals of 10. Data are pooled to include all years (1974–86) and seasons.

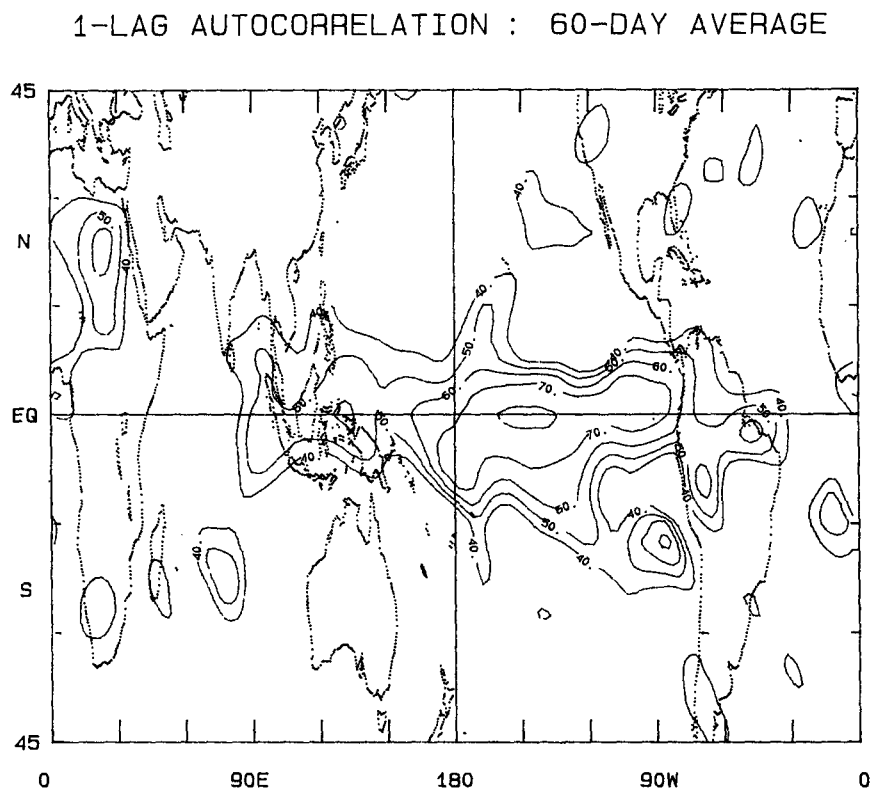

FIG. 1. (*Continued*)

the one-day autocorrelation is the largest, the 60-day autocorrelation is also quite high. In these areas, where 30–60 day oscillations are prevalent, the monthly time scale (anything between 10 and 50 days) should be avoided in simple, local persistence forecasting.

b. Pattern correlations

Autocorrelation maps give an indication of areas that are characterized by large persistence, but it is equally interesting in terms of forecasting to consider spatial pattern correlations (defined in appendix B). Since the areas with the largest departures from the mean, and therefore the largest standard deviations, are normally thought to be the most important regions for forcing remote circulation anomalies, the subsequent results presented here are focused on those regions. In particular, we limit ourselves primarily to the domain from 10°N to 10°S, 90°E to 120°W (the Indo–Pacific domain), which includes areas of large standard deviation on all time scales. Additionally, this domain includes regions which are believed to exert an effect on the Northern Hemisphere midlatitudes, at least during Northern Hemisphere winter (Horel and Wallace 1981; Simmons et al. 1983). The correlations using this domain were found to be slightly larger than when the domain was expanded in the meridional direction.

The full curve in Fig. 3 is a time series of pattern correlations in the Indo–Pacific region using adjacent, nonoverlapping two-month averages that are calculated at monthly increments (i.e., January–February correlated with March–April, February–March with April–May, etc). Most of the values are positive, although there is a large variability of the coefficients, indicating that persistence varies greatly over the 1974–86 period. For comparison, the dashed line in Fig. 3 is the root mean square (rms) of the anomalies over the domain averaged over both the two-month averages from which the correlation map was calculated. There are some episodes during which the persistence is quite large for an extended time. The most apparent of these is during 1982–83. Of course, this persistence coincides with the famous ENSO event, which was associated with enormous OLR anomalies (high rms) in the tropical Pacific. Clearly, this event contributes significantly to any temporal averaging of pattern correlation coefficients.

The full curve in Fig. 4 is a graph of the average one-lag pattern correlation over all years and seasons over the Indo–Pacific domain for many different time averages. For example, the temporally averaged pattern correlation made from two-month averages in Fig. 3, 0.44, nearly corresponds to the full curve in Fig. 4 at 60-day averages. As a matter of record, Fig. 4 was produced by recalculating the averages at three day incre-

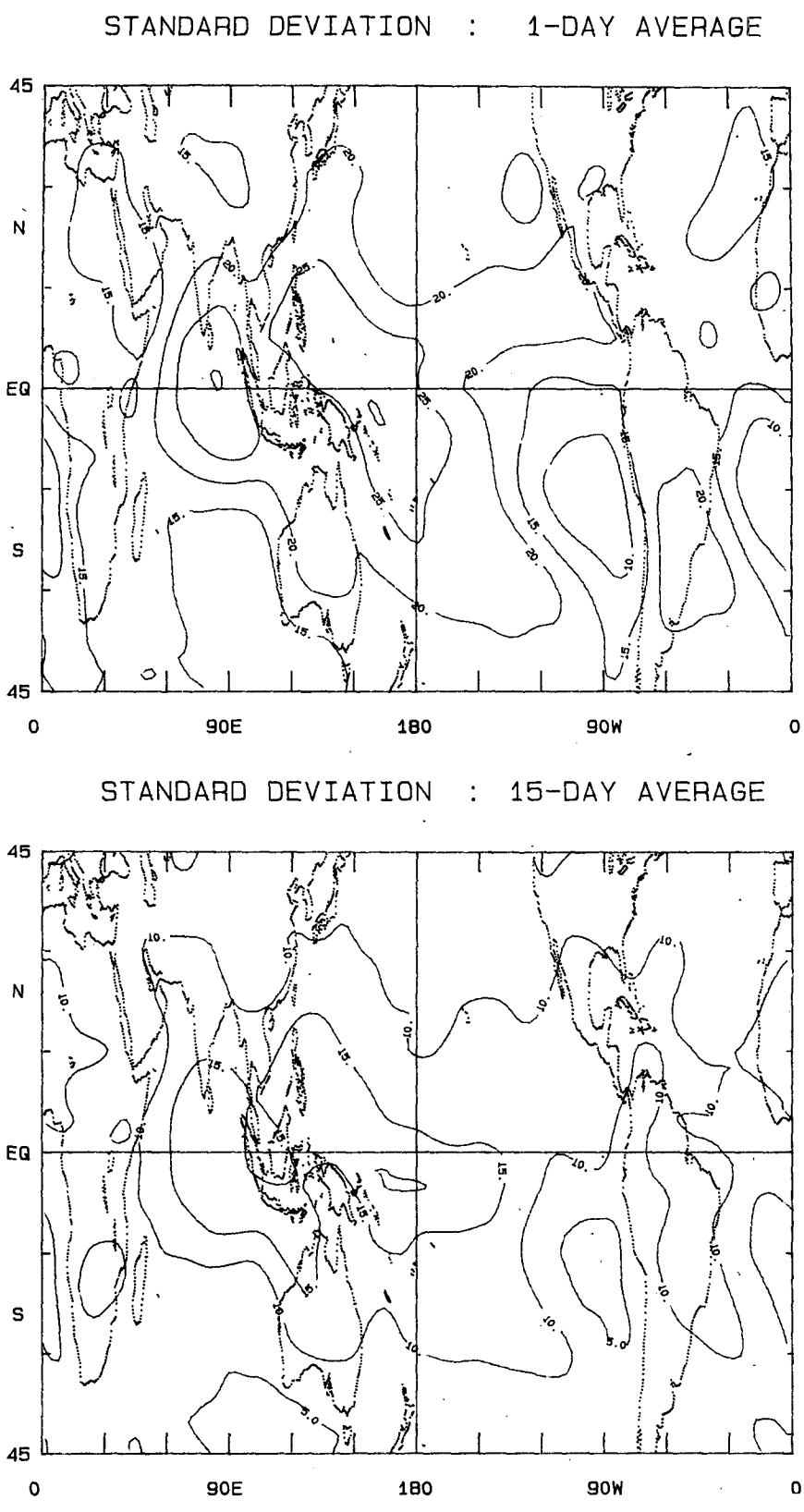

FIG. 2. Standard deviation of OLR based on anomalies from the seasonal cycle for (a) 1-day, (b) 15-day, (c) 60-day averages. Contours are plotted at intervals of 5 W m^{-2}. Data are pooled to include all years (1974–86) and seasons.

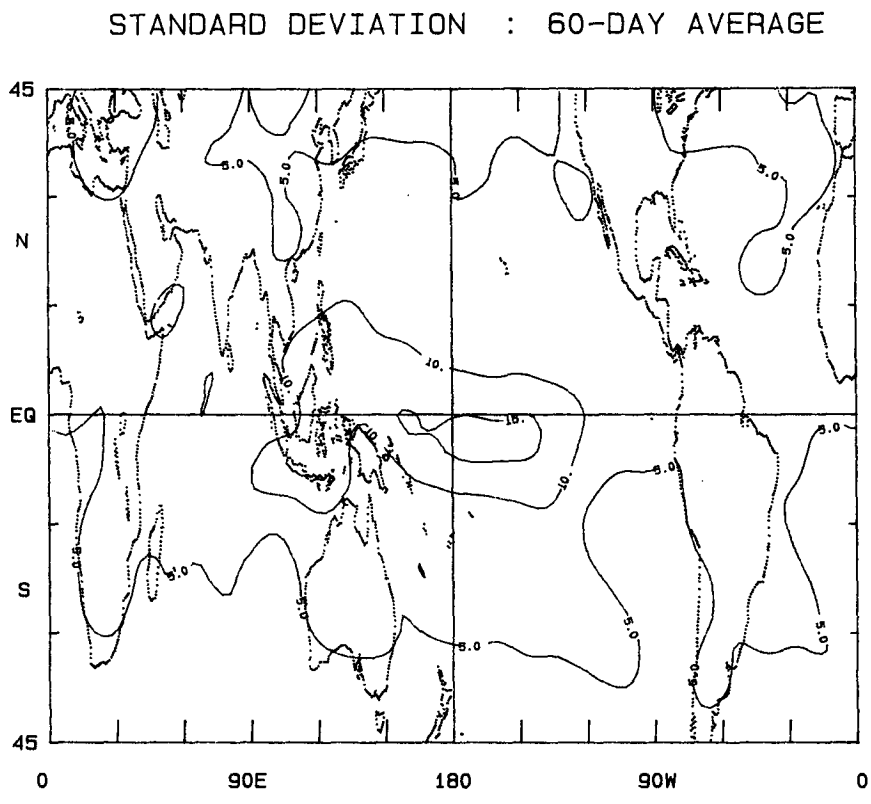

FIG. 2. (*Continued*)

ments rather than using consecutive averages, thus yielding more than 1500 realizations for every averaging period (not all independent). The "sampling frequency" used in producing each graph will be noted in the lower right corner of this and subsequent figures.

One-lag pattern correlations in Fig. 4 (full curve)

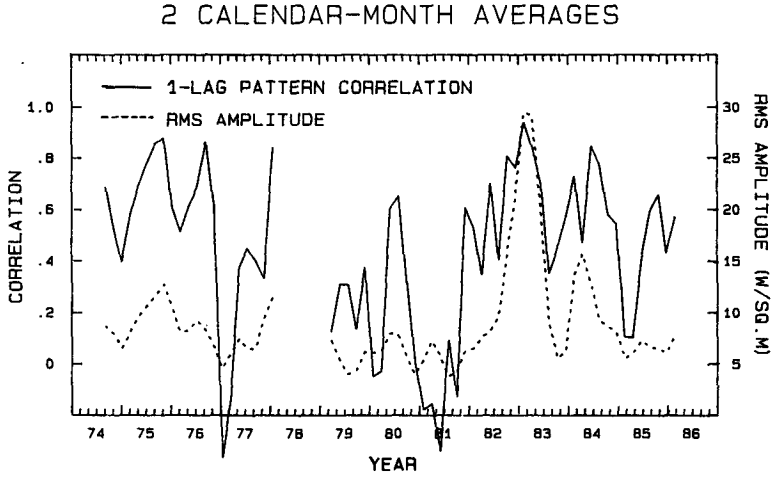

FIG. 3. One-lag pattern correlation (solid curve) plotted as a function of time for a domain extending eastward from 10°N to 10°S, 90°E to 120°W. Lag-correlations are based on adjacent, non-overlapping, two calendar-month averages. Correlation scale is on left side of diagram. Dashed curve is spatial root mean square amplitude of anomalies averaged over the two bi-monthly averages. The rms scale is on right side of diagram in W m^{-2}.

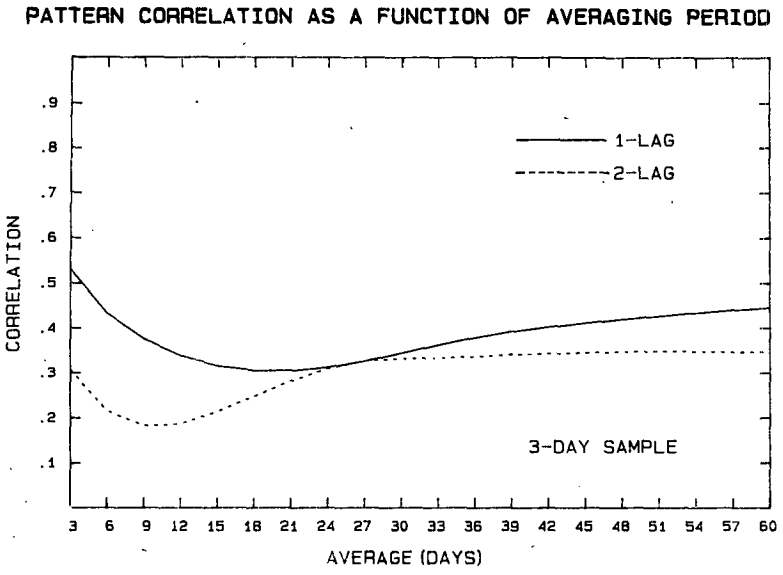

FIG. 4. Average one-lag pattern correlation (solid curve) for all seasons and years as a function of averaging period. Dashed curve is average pattern correlation at two lags.

decrease rapidly with averaging period to a broad minimum near 20-day averages. Then the correlations increase slowly as the averaging period increases further, so that the one-lag correlations using 60–day averages are about as high as those using 6-day averages. The pattern correlations shown by this curve are roughly consistent with the temporal correlations shown in map form in Fig. 1.

The dashed curve in Fig. 4 is the two-lag pattern correlation for the same averaging periods as the upper curve. The correlations are generally smaller at two lags except near averages of 25 days, where the one- and two-lag correlations are equal.

The one- and two-lag pattern correlations both suggest the important contribution of intraseasonal variability with periods between 30 and 60 days in the Indo–Pacific region (Madden and Julian 1971; Weickmann et al. 1985; Lau and Chan 1986) to the total variability in the tropics. The minimum at 20-day averages for one lag and near 10-day averages for two lags both imply an oscillation that is out of phase with the initial anomaly after (on the average) about 20 days.

One-lag average pattern correlation coefficients as a function of month are shown in Fig. 5. The month into which an individual pattern correlation falls is defined as that of the last day of the leading average. It is apparent that the one-day patterns (Fig. 5a) remain large (0.7–0.8) all year, although it appears that slightly larger correlations occur from December through March.

Although the curves using 15- and 60-day averages (Figs. 5b and 5c) do not vary smoothly throughout the year, the average correlation coefficient using 60-day averages is larger in almost every month than the correlations using 15-day averages. The correlations using 60-day averages appear to increase slightly during midyear, meaning, for example, that on the average, the persistence for the two months following July is slightly larger than for the two months following December. It is interesting that while 60-day persistence is generally largest in the midyear months, the 1-day persistence shows a modest minimum during these months.

c. The systematic propagation of OLR anomalies

While there is a certain amount of persistence at all time scales, it is possible that forecasts of OLR anomalies could be improved over pure persistence by taking into account the systematic propagation of large-scale OLR anomalies. Weickmann et al. (1985), Lau and Chan (1985), Liebmann (1987), and others have demonstrated that large-scale OLR anomalies propagate eastward along the equator. This propagation explains in part the relative failure of local persistence (discussed above) in certain areas at time scales from 10 to 40 days.

Diagrams are shown in Fig. 6a that clearly reveal the systematic propagation of OLR anomalies at certain base grid points. These diagrams are like Hovmöller diagrams in that time increases downward along the ordinate and the abscissa represents longitude along the equator. A base grid point at 60 degree increments of longitude is correlated with every grid point along the equator (each value is actually an average between 10°N and 10°S) at varying time lags. Figure 6b is the

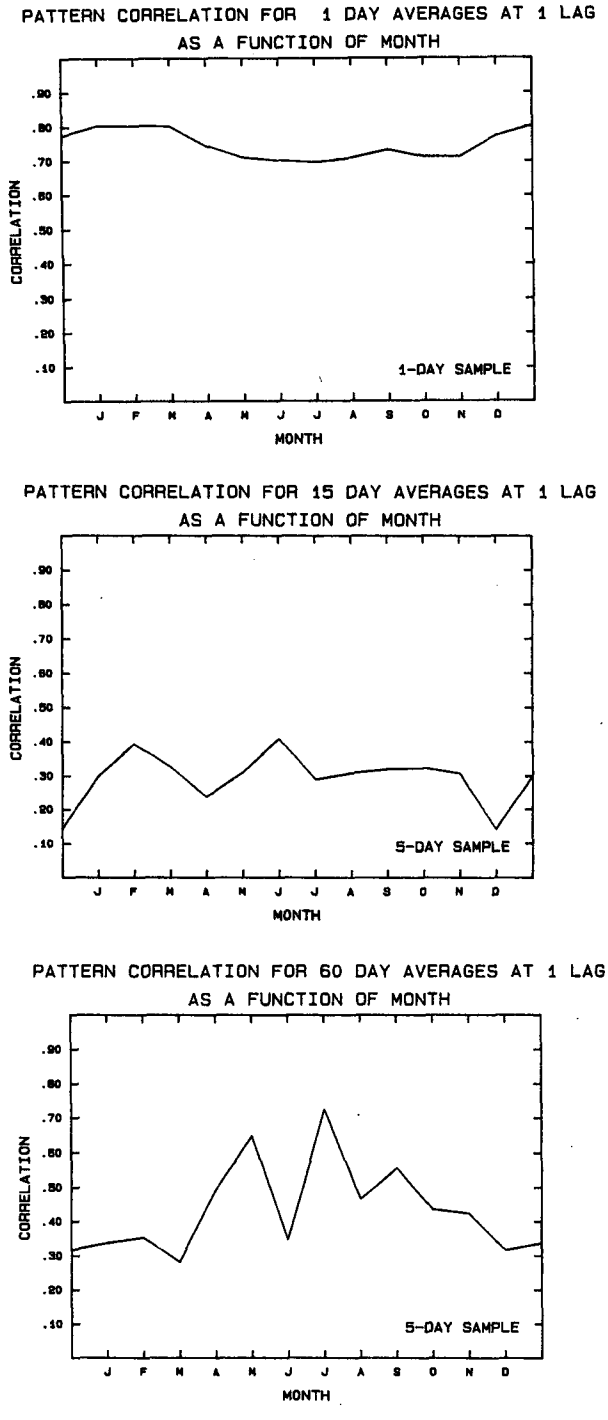

FIG. 5. Average pattern correlation as a function of month for (a) 1-day, (b) 15-day, (c) 60-day averages. Month is attributed to the last day of the leading average.

same as Fig. 6a except that the base grid points are offset by 30 degrees. The correlation coefficient between the base grid point and all other grid points along the equatorial belt, but one day in advance, is plotted at the first tic-mark above the center of the diagram. Thus the contours above the centerline represent OLR anomalies leading the base grid point, and the contours below the centerline represent anomalies lagging behind it. Only positive correlation coefficients are plotted since the negative correlations are weak in all cases (never less than −0.3) and do not aid in our description of phase propagation. Since significant values are relatively local, more than one base grid point has been plotted on each diagram. In Fig. 6, the correlations are plotted alternately as dashed and solid lines to avoid confusion. The diagrams are based on daily averages and all seasons are pooled. Propagation speed of the anomalies is determined by the degree to which the axis of maximum correlation is tilted (see subjectively drawn phase propagation lines).

There are at least three time scales of eastward propagation[2] evident in Fig. 6. OLR anomalies between 60° and 120°E appear to propagate about 30 degrees eastward from day −12 to day +12, corresponding to a phase speed of approximately 1.5 m s^{-1}. Interestingly, Lau and Chan (1985) and Weickmann et al. (1985), in their studies of *intraseasonal* variability of OLR in the tropics during Northern winter, found an eastward phase speed of about 5 m s^{-1} in this region. OLR anomalies at several other base points, however, appear to exhibit a much more rapid phase speed, traversing about 20 degrees of longitude in two days. The clearest example of this rapid phase propagation is at the prime meridian. Finally, grid points over the eastern Pacific (180°–120°W) exhibit large persistence upon which is imposed a rapidly eastward propagating anomaly. The persistent component is mostly due to the 1982–83 ENSO, which produced long-lived anomalies of unprecedented magnitude, but at the dateline there is also a contribution from stalling 30–60 day waves (Lau and Chan 1985).

Since eastward propagation is evident at most longitudes, it is possible that a multiple regression approach could increase the skill in forecasting OLR anomalies near the equator over that obtained by persistence alone. This can be done either by a regression involving all grid points at various antecedent time levels, or, more efficiently, by regressing on time series of coefficients of complex empirical orthogonal functions of the OLR anomalies.

The pronounced eastward propagation evident between 60° and 120°E occurs primarily with periods between 30 and 60 days (Weickmann et al. 1985). It is therefore likely that if anomalies were to be forecast using the regression approach, the most improvement would be evident in frequencies corresponding to those periods. Although the line of maximum correlation exhibits a tilt at most longitudes, implying a systematic eastward propagation of OLR anomalies, the maximum correlation at any given lag is almost always at

[2] There is almost no evidence for westward propagation of anomalies, except possibly at 30°W.

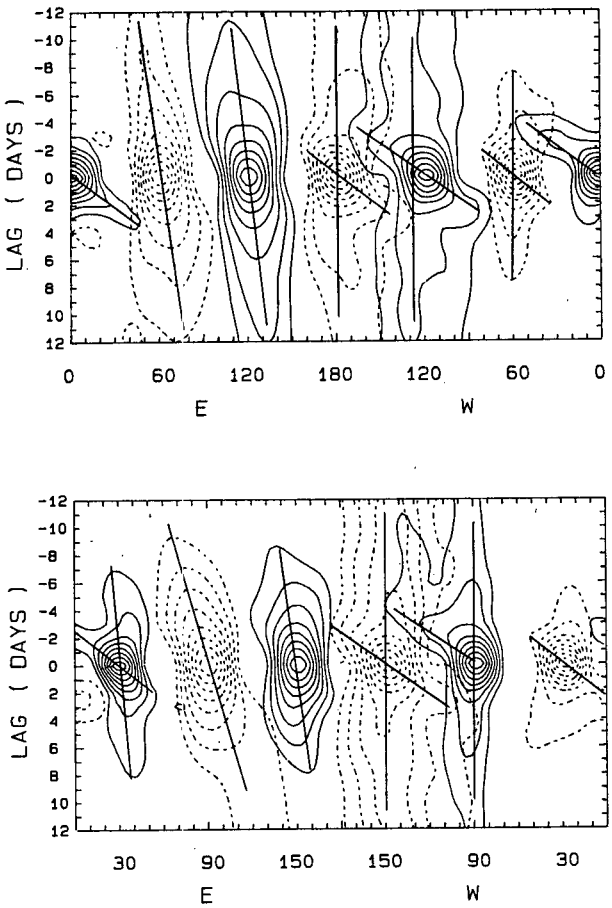

FIG. 6. (a) Correlation between base grid points and every grid point in equatorial strip that leads or lags base grid point by number of days noted on left side of diagram. Correlations are plotted for base grid points at 60 degree increments of longitude. Contour interval is 0.1, starting at 0.2. Only positive contours are plotted. Correlations surrounding base grid points are plotted alternately as dashed and solid curves. The input OLR anomalies are meridionally averaged between 10°N and 10°S. Lines of phase propagation are subjectively drawn. (b) As in (a) except that the base grid points are shifted by 30 degrees.

the base grid point due to the quasi-circular pattern of correlation, thus entering persistence as the first term in a regression equation.

4. Summary

In this paper we have investigated the persistence of OLR anomalies in the tropics at many different time scales. Persistence forecasting is dependent on region, averaging period, the state of the climate system (e.g. ENSO or no-ENSO), and, to a lesser extent, the season.

Autocorrelations made with 1-day averages are typically large near the equator and decrease towards midlatitudes. Autocorrelations made with 15- and 60-day averages have their largest values over the equatorial Pacific east of the dateline, where they are at least as large as autocorrelations made with 1-day averages. With the 60-day averages, relatively large values extend westward into the Indian Ocean, a feature not evident using 15-day averages. We believe the westward extension is not seen on the 15-day average maps because of the presence in this region of oscillations with periods between 30 and 60 days. Areas of large standard deviation are not well matched with those of large autocorrelation, especially at 15-day averages.

We calculated pattern correlation coefficients for an area from 10°N to 10°S, 90°E to 120°W. Using adjacent, nonoverlapping, two calendar-month averages, the coefficients are generally positive, but are highly variable with time. There are a few distinct episodes of large persistence, most notably during the 1982–83 ENSO event. These few events contribute significantly to the average "forecast skill."

On the average, the pattern correlations decrease with increasing averaging period to a minimum at about 20-day averages. Then they increase slowly so that the average pattern correlation using 35-day averages is about the same as that using 10-day averages.

There is evidence of weak seasonality in the average pattern correlation. The one-day correlations show a slight minimum during the midyear months, while pattern correlations made using 60-day averages seem to increase during midyear. Finally, we showed systematic eastward propagation of large-scale OLR anomalies, and suggested that it may be possible to improve forecasts over simple, local persistence by a multiple regression scheme.

It has been demonstrated elsewhere that there is at least some skill in predicting midlatitude circulation anomalies with a knowledge of the simultaneous tropical OLR distribution, even with a linear dynamical model (e.g., Mureau et al. 1987; Chelliah et al. 1988). It would therefore be useful to develop a set of regression equations to prognosticate tropical OLR anomalies. Eventually, of course, one would hope that tropical OLR anomalies could be predicted dynamically, but until then, the regression approach could be quite useful.

It would also be useful if we could identify in advance those tropical circulation regimes that are likely to be persistent. Then at least one could forecast with confidence in certain situations. It is these highly persistent situations that are likely to have the most effect on the midlatitude circulation.

Acknowledgments. We wish to thank Dr. J. S. Winston for sharing his earlier work on the subject that motivated our research, and Professor J. M. Wallace for suggesting the time–longitude correlation diagram. The work was supported by the Cooperative Institute for Climate Studies under NOAA Grant NA84-AA-H-00026. Some of the manuscript was written while the first author worked at the Cooperative Institute for Research in Environmental Sciences, University of Colorado.

APPENDIX A

Computing Anomalies

We first computed calendar-month normals from all available OLR data and then subjected the 12 values at each gridpoint to a Fourier analysis, retaining the annual and semiannual harmonics and the mean. We then assigned a value to every day of the year, and subtracted these values from the appropriate day of the record.

Of course, the most obvious way to calculate a climatology is to subject the daily normals to a Fourier analysis. To ease computing requirements, however, we deemed our method as adequate.

The ratio of the amplitude of the harmonics generated by using 30-day means to that using daily means (the true amplitude) is expressed as:

$$\frac{\text{monthly}}{\text{daily}} = \frac{\sin(30\pi f)}{30\pi f},$$

where $f = 1/365$ and $2/365$ for the annual and semiannual harmonics, respectively. The ratio for the first and second harmonics, therefore, is 0.989 and 0.956, respectively.

In our data the first harmonic explains an average of 92.4% of the variance of the monthly climatology and the first two together explain 96.5%, thus yielding a smooth, fairly complete, and inexpensively obtained climatology.

APPENDIX B

Definitions

Autocorrelation:

$$\mathrm{AC}(i,\tau) = \frac{\sum_t \hat{R}_i(t)\hat{R}_i(t+\tau)}{[\sum_t \hat{R}_i^2(t) \sum_t \hat{R}_i^2(t+\tau)]^{1/2}}, \quad (1)$$

where $\hat{R}$ is the anomaly from the long term climatology (see appendix A), i is the grid point index, t is time, and τ is the lag; AC is a function of lag and space.

Pattern correlation:

$$\mathrm{PC}(t,\tau) = \frac{\sum_i \hat{R}_i(t)\hat{R}_i(t+\tau)}{[\sum_i \hat{R}_i^2(t) \sum_i \hat{R}_i^2(t+\tau)]^{1/2}}; \quad (2)$$

PC is a function of lag and domain.

Notice that in Eq. (2) the spatial mean of $\hat{R}$, nonzero in general, is not removed from either the numerator or denominator (Horel 1985). In (1), the temporal mean is zero by definition.

To study the spatial distribution of persistence AC is the best tool; to study the seasonality in persistence PC is appropriate.

The summation over t in (1) can be performed over a desired season or the whole year. Likewise in (2), the summation over i can be performed over subareas or the entire globe.

When we correlate time averages (of $\hat{R}$) in this paper the lag τ is a multiple of the time average. For example, lag one for 30-day averages implies a lag of 30 days (measured between the centers of the two averages).

REFERENCES

Chelliah, M., J. E. Schemm and H. M. van den Dool, 1988: On the impact of low-latitude anomalous forcing on local and remote circulation: Winters (DJF) 1978/79–1986/87. *J. Climate,* **1,** 1138–1152.

Horel, J. D., 1985: Persistence of the 500 mb height field during Northern Hemisphere winter. *Mon. Wea. Rev.,* **113,** 2030–2042.

——, and J. M. Wallace, 1981: Planetary scale atmospheric phenomena associated with the Southern Oscillation. *Mon. Wea. Rev.,* **109,** 813–829.

Lau, K.-M., and P. H. Chan, 1985: Aspects of the 40–50 day oscillation during the Northern winter as inferred from outgoing longwave radiation. *Mon. Wea. Rev.,* **113,** 1889–1909.

——, and ——, 1986: The 40–50 day oscillation and the El Niño/Southern Oscillation: A new perspective. *Bull. Amer. Meteor. Soc.,* **67,** 533–534.

Liebmann, B., 1987: Observed relationships between large-scale tropical convection and the tropical circulation on subseasonal time scales during Northern Hemisphere winter. *J. Atmos. Sci.,* **44,** 2543–2561.

Madden, R. A., and P. R. Julian, 1971: Detection of a 40–50 day oscillation in the zonal wind in the tropical Pacific. *J. Atmos. Sci.,* **28,** 702–708.

Mureau, R., J. D. Opsteegh and J. S. Winston, 1987: Simulation of the effects of tropical heat sources on the atmospheric circulation. *Mon. Wea. Rev.,* **115,** 856–870.

Roads, J. O., and T. P. Barnett, 1984: Forecasts of the 500 mb height using a dynamically oriented statistical model. *Mon. Wea. Rev.,* **112,** 1354–1369.

Simmons, A. J., J. M. Wallace and G. W. Branstator, 1983: Barotropic wave propagation and instability, and atmospheric teleconnection patterns. *J. Atmos. Sci.,* **40,** 1363–1392.

Van den Dool, H. M., and R. M. Chervin, 1986: A comparison of month-to-month persistence of anomalies in a general circulation model and in the Earth's atmosphere. *J. Atmos. Sci.,* **43,** 1454–1466.

Weickmann, K. M., G. R. Lussky and J. E. Kutzbach, 1985: Intraseasonal (30–60 day) fluctuations of outgoing longwave radiation and 250 mb streamfunction during Northern winter. *Mon. Wea. Rev.,* **113,** 941–961.